Egyptian Journal of Chemistry
http://ejchem.journals.ekb.eg/

Modelling of the dynamic behavior for Lead-Acid Batteries in photovoltaic systems

R. M. Abdo [a], Aiat Hegazy [a*], E. T. El Shenawy [a], and E. F. El-Sherbini [b]
[a] Solar Energy Department, National Research Center, Cairo, Egypt
[b] Chemistry Department, Faculty of Science, Ain Shams University, Cairo, Egypt

In Loving Memory of Late Professor Doctor ""Mohamed Refaat Hussein Mahran""

Abstract
To enhance a photovoltaic system's performance, it is important to understand the electrical characteristics of its main components: photovoltaic modules and batteries. Models can simulate these components, but often require knowing specific parameters. Batteries are most complex as they alone deviate from ideality. The performance of batteries is primarily influenced by various factors such as electrolyte concentration, temperature, internal resistance, charging/discharging rate, and state of charge. Therefore, it is crucial to accurately understand battery behavior throughout operation. While electrolyte concentration is the most effective indicator of state of charge, it is difficult to measure directly in photovoltaic systems. Thus, voltage can be considered a good indicator of state of charge and battery behavior. Understanding battery behavior is vital for accurate modeling.
Models' electric characteristics were assessed and derived as functions of state of charge using curve fitting to represent real performance without simplicity loss. This paper compares the improved Thévenin model to the Partnership for a New Generation of Vehicle (PNGV) model for 200 Ah lead-acid batteries. It also aims to link battery capacity/state of charge accurately to voltage by validating PNGV's 3% root-mean-square error (RMSE). While modifying Thévenin expressed dynamics, it did not fit the data below 50% state of charge appropriately. PNGV experimentally validated for real-time use discharging to 20% state of charge, accurately expressing behavior across the range.
Keywords: lead acid battery; Equivalent circuit model; PNGV model; Thévenin model; Discharge mode.

1. Introduction

The provision of electricity has recently turned into a necessity for the ongoing survival and growth of emerging communities. Promoting the use of alternative energy sources, like solar energy, has been promising especially when considering Egypt's high levels of radiation. Photovoltaic systems are the most favorable environmental-friendly sources constructed to fulfill worldwide energy requirements for various applications [1]. One challenge created by these systems is that they are highly affected to both the weather variations and fluctuations in the electricity demand. Solar collectors output electricity only during the sunshine period [2].

A storage unit is the choice for achieving a balance between the generation of electricity and its use [3]. Consequently, the core components for any PV system are Batteries as the storage unit.

Lead-acid batteries have become a mature technology and are widely used in various applications [4-9]due to their low cost, high availability, and ease of manufacturing. They remain the predominant energy storage and delivery devices used in photovoltaic (PV) systems[6, 7]. Lead-acid batteries come in a variety of designs, sizes, and voltages to meet different needs. Developments have yielded maintenance-free models that can operate in any orientation. To satisfy changing requirements, two lead-acid battery types emerged. Sealed lead-acid (SLA, also called gel cell) batteries and valve-regulated lead-acid (VRLA) batteries replaced traditional liquid electrolytes with moistened separators and added safety valves to vent gasses during charging and discharging [10-13].

A lead-acid battery's dynamic behavior depends on its state of charge, charging/discharging rates, and temperature [14-17]. Modeling these dynamics is complex, as is determining model parameters. The difference between electromotive force and terminal voltage stems from polarization effects, including ohmic voltage drop and overvoltage. Ohmic drop results from resistances in active materials, electrode grids, and porous separators. Overvoltage represents the extra energy needed for electrochemical reactions

* Corresponding author: aiathussien@gmail.com.
Receive Date: 10 December 2023, Revise Date: 02 January 2024, Accept Date: 10 January 2024
DOI: 10.21608/ejchem.2024.254444.8973

to proceed at desired rates. Thus, the battery voltage is expressed as follows:

$$V = V_o + I \times R \qquad (1)$$

Where, V is the battery voltage during charge or discharge, V_o is the open circuit voltage at steady state; R is the internal resistance of the battery. I is the current passes from and to the battery. During discharge, the current has a negative value, indicating the flow of current out of the battery. Conversely, during charging, the current has a positive value, indicating the flow of current into the battery.

Polarization varies with state of charge, current flow, temperature, and operating mode [16, 17]. Depth of discharge also affects performance deviations from ideal behavior. High-discharge applications subject batteries to partial state of charge cycling without full recharging, allowing sulfation to predominate. This forms large lead sulfate crystals that block active sites, decrease efficacy, and accelerate failure[18]. Consequently, terminal voltage is always lower than electromotive force during discharge but higher during charging.

Due to these dynamics, modeling and parameter determination involve complex processes. Battery models can be classified by perspective (electrochemical, electrical, thermal, mechanical, interdisciplinary, depth, or technique [19-21]. Equivalent circuit models (ECMs) are widely used for modeling, simulation, and state of charge estimation [14, 15] without requiring an in-depth understanding of chemical mechanisms. They also avoid computational complexity by using a few easily measured electrical variables [22]. Over decades, ECMs for lead-acid batteries have undergone significant development. Techniques like neural network-based learning [23-25] and incorporating open circuit voltage as a state of charge predictor were crucial for enhancing dynamic performance [26-28]. Using the nonlinear relationship between state of charge and open circuit voltage further improved models [29]. ECM element parameter values are defined as constants, lookup tables, or fitted functions of state of charge and temperature [30].

The simplest ECM was introduced as a linear model by Kim and Ha [31]. Numerous proposals followed, including the common Thévenin ECM (Figure 1) providing a straightforward representation of battery voltage (U_b). It incorporates no-load voltage (UOC), internal resistance (R_o), and battery overvoltage (represented by a parallel capacitor-resistor combination, $R_{ov}//C_{ov}$). However, these values are not truly constant but vary with state of charge, capacity, charge/discharge rates, age, and temperature. Therefore, a more comprehensive model was developed to accurately capture lead-acid battery dynamic performance [16, 31].

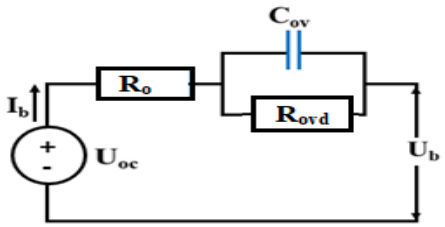

Figure 1: Thévenin equivalent circuit model.

An enhanced Thévenin battery model has been created to provide a more accurate portrayal of battery behavior through accounting for nonlinear characteristics dynamically [16, 32, 33]. This advanced model characterizes the internal resistance, self-discharge resistance, and overcharge resistance as variables dependent upon the state of charge. Additionally, the charging and discharging processes are separately defined, as delineated in Figure 2. This nuanced approach offers heightened fidelity compared to predecessor models that treated parameters as static [16, 32, 33]. By embracing nonlinearity and distinguishing charging from discharging, the improved model offers a more robust framework for simulating real-world battery performance over diverse operating conditions [14, 34, 35].

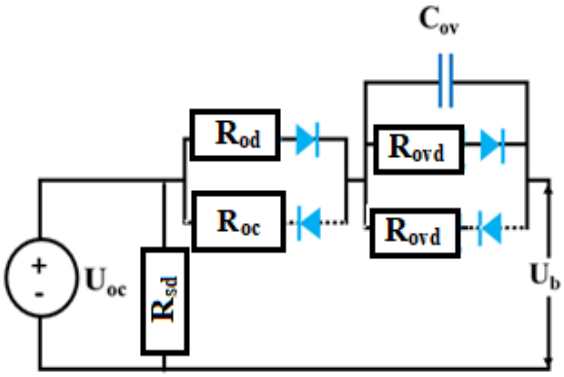

Figure 2: Improved Thévenin model for Lead acid battery.

To better model the kinetic voltage behavior of batteries (such as charge transfer, diffusion within electrodes and electrolytes, ion migration, and concentration gradients), improved "dynamic" equivalent circuit models (ECMs) incorporate additional electric circuit elements like resistors, capacitors, and conductors [34, 36]. It is a common practice to include multiple parallel resistor-capacitor (R-C) combinations to satisfactorily represent the voltage behavior. However, relying solely on two R-C elements may not adequately capture the diverse range of voltage loss effects, in addition to computational costs considerations.

As batteries can be considered analogous to real capacitors serving as electrical energy storage, the stored charge amount can be described by the state of charge (SOC). Accordingly, some modification approaches involve a large series capacitance (C), such as the so-called Partnership for a New Generation of Vehicle (PNGV) model type. This model (illustrated in Figure 3) includes an open-circuit voltage (U_{oc}), a high-value series capacitor (C_o), and a resistor (R_o), in addition to a parallel combination of R_{ov} and C_{ov}. The model aims to depict voltage variations through stored or depleted charges, specifically modeling Faradaic processes that account for battery electrochemistry simulations [14, 37].

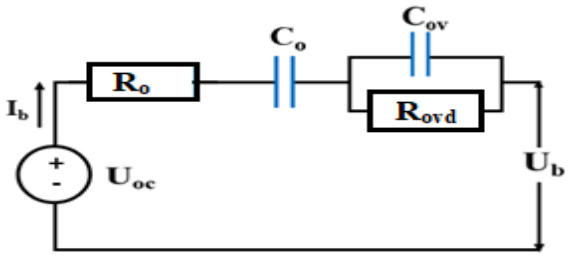

Figure 3: Equivalent circuit of the PNGV model.

This study will conduct a comparative analysis of the modified Thévenin and PNGV battery models. The analysis will include an evaluation of the model parameters and validation of each model using experimental data from a 200 Ah lead-acid battery. Validation will also utilize the manufacturer's technical specifications.

The modified Thévenin and PNGV models will be simulated and compared to experimental discharge curves obtained for discharge rate of C/20. Model parameters will be extracted by fitting the simulations to the experimental data. Key metrics like capacity, internal resistance and voltage characteristics will be evaluated and compared between the two models and experimental results. Model accuracy and robustness will be assessed based on parameter estimation errors and goodness of fit statistics.

The results will provide insights into the most suitable modeling approach for the given battery specifications and intended application. With accurate modeling, optimal control and utilization strategies can be developed for maximizing service life and performance of lead-acid batteries in stationary energy storage systems.

2. Methods

This section will outline the methodology, experimental protocols, and model validations using real battery data.

3. Experimental Set-up

Parameters for the equivalent circuit models (ECMs) were determined through pulse-discharge testing of a lead acid battery within a state of charge (SOC) range of 100-20%. The battery under examination is a gel-type lead-acid battery with a nominal capacity of 200 Ah at the C/20 discharge rate and a nominal voltage of 12 V.

Batteries were charged through a photovoltaic system (shown in Figure 4) consisting of:

• 2-solar panels 140 W Sunset 1406 (I_{sc} 8.3 A, V_{oc} 21.8 V) and

• TAROM 4545 charge controller [12/24 V– 45 A]

• 12 V, 0.6 kW SUVPR inverter; converted the direct current to alternating current.

3.1. Discharging methodology:

Before starting discharging process, the battery was charged to approximately 100% state of charge via the solar panels during daytime (8am-3pm) at current range of (6-9 A) and allowed to rest for 24 hours before testing commenced. Discharging processes were operated used AC electric lamps with 120 W.

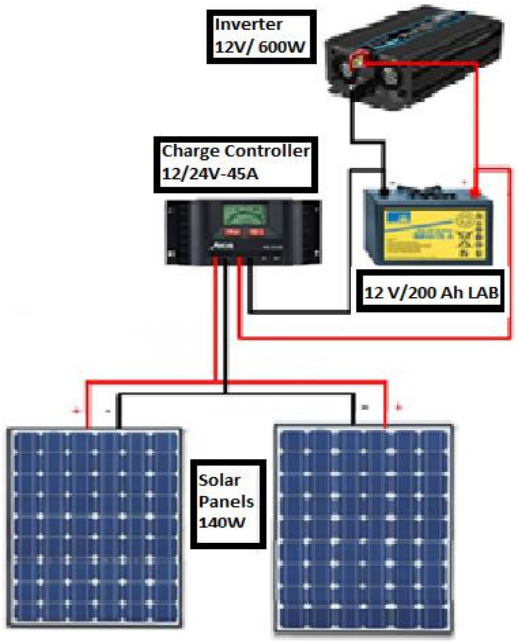

Figure 4: Schematic diagram for Solar PV system

3.2. Model Validation using Real Battery Data

The battery modeling equations are primarily carried out in terms of the SOC, and the battery terminal voltage equation is determined according to the equivalent circuit of the tested models. The state of charge is quantified as a percentage as follows [32]:

$$SOC = SOC_o + \left[\frac{1}{C_n}\int_0^t \pm I_b\,,dt\right] \times 100 \qquad (2)$$

Where SOC_o represents the initial state of charge in percentage, C_n indicates the nominal capacity in amp-hours, I_b denotes the battery current in amperes, which is considered positive during charging and negative for discharging, and t represents the charge or discharge time.

The parameters for these ECMs were determined through a pulse-discharge test conducted within a SOC range of 100-20%. For simplicity, the circuit parameters will be elucidated for only one discharge rate, C/20, presented in Figure 5. Figure 5a represents the battery voltage measured during discharge pulse tests performed according to the sequence: 15-minute discharge with a current of I_b= 10 A, followed by a 45-minute recovery period. Figure 5b highlights both the diffusion control (concentration-polarization) region in addition to the steady state region upon pulsed discharging of the battery. Figure 5b magnifies the battery terminal voltage during different distinct stages; the discharge pulse intervals, and rest interval. According to Figure 5b, the rest interval is divided into three stages:

The first stage, named as IR jump, represents the rapid increase in potential just after removing the load and reflects the effect of internal resistance or R_o.

The second stage, denoted as U_{ov}, represents the gradient increase in potential and reflects the diffusion effect represented by a parallel capacitor-resistor combination, $R_{ov}//C_{ov}$.

The third stage represents the open circuit voltage at the steady state.

4. Results and Discussion

4.1. The improved Thévenin model

The first model presented is a dynamic approach to understanding lead-acid batteries, as an expansion of the Thévenin model that considers the nonlinear behavior of the electric parameters of the overvoltage processes, represented by an overvoltage capacitor in parallel with a single polarization resistor. The terminal voltage (Ub) is expressed according to equation 3.

$$U_b = U_{oc} - I_b R_o - U_{ov} \qquad (3)$$

$$U_{ov} = I_b R_{ov}.\left[1 - e^{\left(-\frac{t}{R_{ov}.C_{ov}}\right)}\right] \qquad (4)$$

Where, U_b represents the terminal discharge voltage, U_{oc} represents the open circuit voltage, and U_{ov} represents the overvoltage across the resistor-capacitor element ($R_{ov}//C_{ov}$). To validate the model, the terminal battery voltage will be simulated through the determination of the parameters of the considered ECM (R_o, R_{ov}, C_{ov}) from pulse-discharge tests. The parameters curves vs. SOC will be fitted, producing equations with SOC that will be incorporated into the corresponding simulation model as follow.

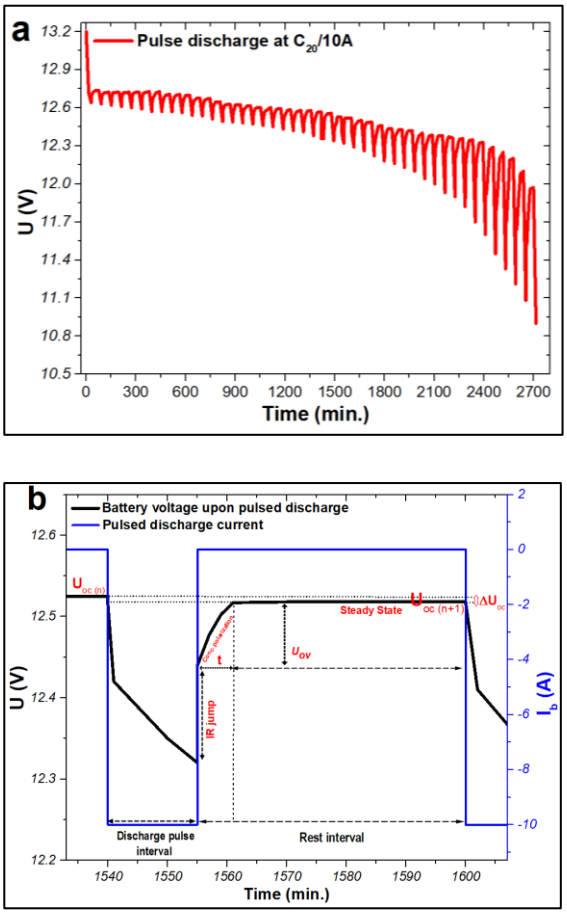

Figure 5: (a) Pulse discharge at C/20/10 A for 200 Ah Lead-acid battery **(b)** the battery terminal voltage and the applied current showing the discharge pulse intervals, and rest interval which include IR shift and the diffusion-controlled region and the steady state region during rest intervals.

4.2. Estimation of model parameters

4.2.1. Self-discharge resistance (R_{sd})

The battery undergoes self-discharge when left for a long period under rest conditions. To configure the self-discharge resistance(R_{sd}), the self-discharge

current (I_{sd}) is calculated from the data of the capacity loss within the storage time at 20°C given by the manufacturer [32], [38]. For A400 Sonnenschein batteries, the self-discharging rate is estimated to be less than 0.05% per day [38]. The self-discharge current I_{sd} at 20°C is assumed to be constant within each interval of the storage time [32]. Consequently, it can be explained as follows:

$$I_{sd} = \frac{\Delta SOC}{100}, \frac{C_n}{\Delta t} \quad (5)$$

ΔSOC is the decrease in the state of charge percentage of the battery when left under rest for time interval Δt, C_n is the rated battery capacity given by the manufacturer. R_{sd} can be estimated from open circuit voltage as follows:

$$R_{sd} = \frac{U_{oc}}{I_{sd}} \quad (6)$$

A plot between R_{sd} values and SOC is depicted in Figure 6 to predict their mathematical relation using curve-fitting technique. The relation between R_{sd} and SOC is fitted by polynomial function and is expressed as:

$$R_{sd} = 3,96 + 0,005 \times SOC - 0,0000216 \times SOC^2 \quad (7)$$

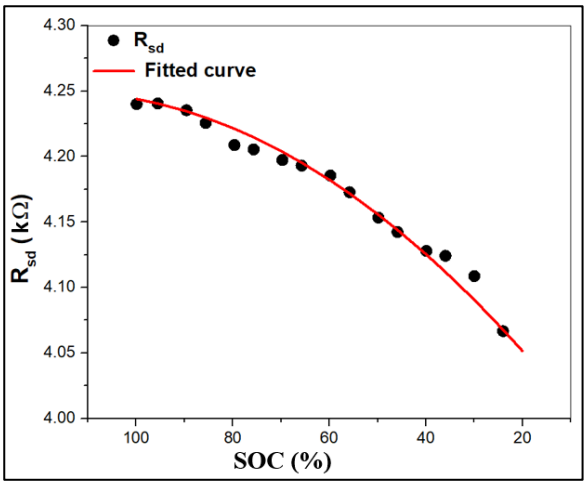

Figure 6: The relation between R_{sd} and SOC

4.3. Open circuit voltage (U_{oc})

The Open Circuit Voltage (Uoc) was measured at the steady state at the end of rest intervals then it was

firstly introduced and fitted as a parameter to be used in both ECMs under investigations. The experimental data were subjected to a quadratic polynomial fitting and a *f* (SOC) according to equation 8

$$U_{oc} = 11.87 + 0.015 \text{ x SOC } -0.000065 \text{ x SOC}^2 \quad (8)$$

The graph of Uoc fitted results (determined from Figure 5, black line, and polynomial fitted, red line) and SOC is shown in Figure 7.

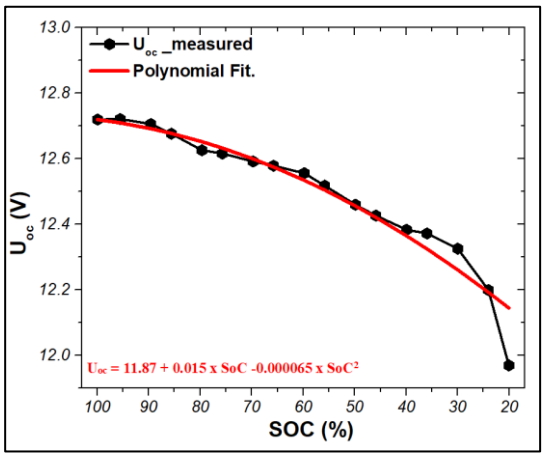

Figure 7: Open Circuit Voltage (U_{oc}) fitting curve with SOC

4.4. Series resistance (R_o):

The parameter denoted as the series resistance (Ro) represents the series resistance determined from the voltage step responses at the end of the discharging intervals as shown in Figure 5b (the first stage in the rest interval)

Figure 8 illustrates the values of Ro as a function of SOC. Notably, series resistance values are constant upon discharging before 45% SOC, showing a significant increase up to 7 folds afterward, reflecting a serious effect of Ro on the battery potential after 40% SOC. This increase is correlated with the increase of the total internal resistance (Ohmic and polarization resistances) accompanied with sulfation phenomenon [18], [29] which commonly occurs in this SOC range. In our study, a reasonably approximation of the experimental values of Ro through exponential fitting was achieved, resulting in f (SOC) equation.

$$R_o = 0,012 + 0,29 \times 0,925^{SOC} \quad (9)$$

4.5. R//C network:

The electrical circuit model incorporates the parallel resistor//capacitor branch (Rov//Cov) to consider the battery's Faradaic processes, which cause deviation in the battery terminal voltage away from its ideal value. This network can be determined from the gradient change in the potential (Uov) during the rest interval as shown in Figure 5b (the second stage) according to Equation 4.

Based on the estimation of the settling time (t) of the voltage response, it is expected that the transients for all discharge rates dissipate within 5 minutes. It is evident that the voltage reduction occurs slower for lower discharge rates, resulting in longer transient intervals [32]. Thus, the time constant (τ) chosen for

this analysis is 1 minute and the concentration overvoltage capacitance (**C_{ov}**) is estimated according to the following equations:

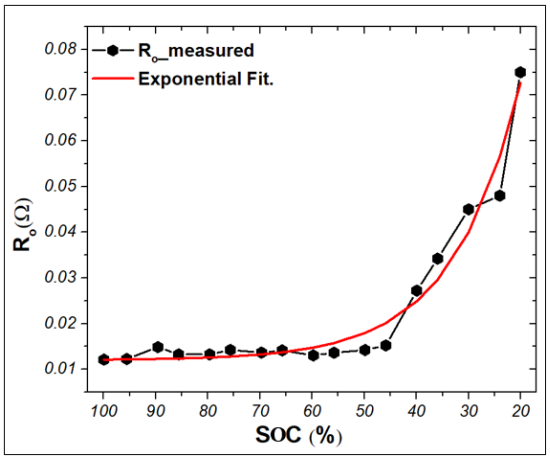

Figure 8: Variation of series resistance (R_o) at different SOC.

$$C_{ov} = \frac{t}{5R_c} = \frac{\tau}{R_c} \qquad (10)$$

R_c depicts the resistance of the battery circuit (**R_o** and **R_{ov}**) and is determined according to the following equation:

$$R_c = \frac{R_o \times R_{ov}}{R_o + R_{ov}} \qquad (11)$$

Using curve-fitting technique, **R_{ov}** and **C_{ov}** can be described as:

$$R_{ov} = 0,009 + 1,95 \times 0,87^{SOC} \qquad (12)$$

$$C_{ov} = -154 + 10,27 \times SOC - 0,09622 \times SOC^2 + 0,0002765 \times SOC^3 \qquad (13)$$

The values of **R_{ov}**, **R_c** and **C_{ov}** are shown in Figure 9.

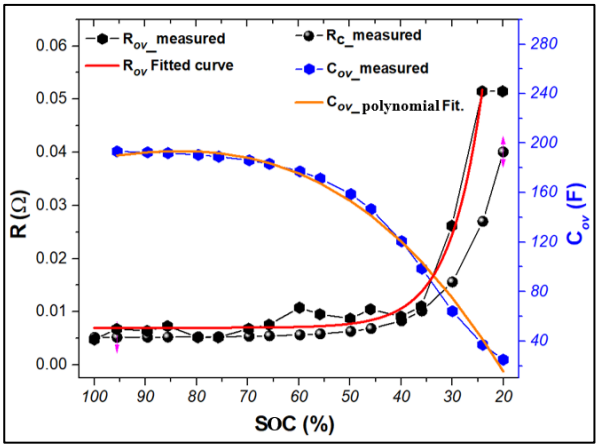

Figure 9: Experimental and fitted values of R_{ov} and C_{ov} as a function of SOC.

- **U_{ov} simulation**

Figure 10 shows the experimental and *f* (SOC) fitted data of **U_{ov}**, expressed in the following equation:

$$U_{ov} = 0.0935 + 18 \times 0.86^{SOC} \qquad (14)$$

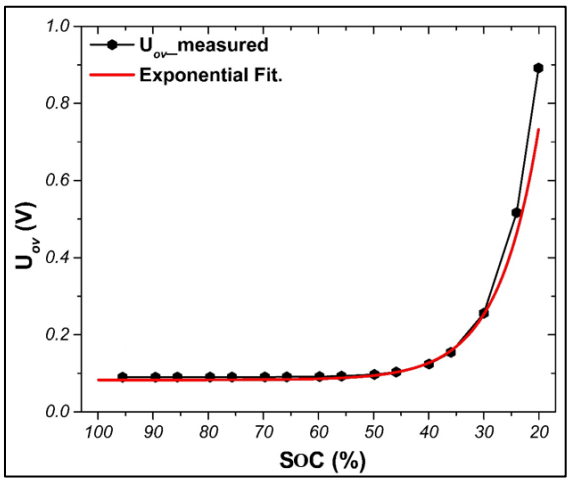

Figure 10: Experimental and fitted values of U_{ov} as a function of the SOC.

4.5.1. Validation of Thévenin model

Figure 11 illustrates the validation results of the improved Thévenin battery model that shows a comparison between the simulated terminal voltage (Ub) and the actual discharge experimental data. The experimental values were remarkably approximated by fitting equations (number 8, 9, and 14) that are dependent on the state of charge (SOC). The remarkable equations were incorporated into the simulation model, for validation of model, matching it with the experimental results. From Figure 11, it seems that the improved Thévenin model cannot entirely simulate non-linear processes and transient response of the battery. This model shows a limitation at low SOC values, and hence, cannot correctly estimate the battery voltage upon discharging. The ECM parameters did not define to represent the battery real performance, limiting the model ability to run in matching the experimental results especially at SOC values less than 40%. The absolute error is presented in the inset inside Figure 11, and the root-mean-square error of this model is around 6%.

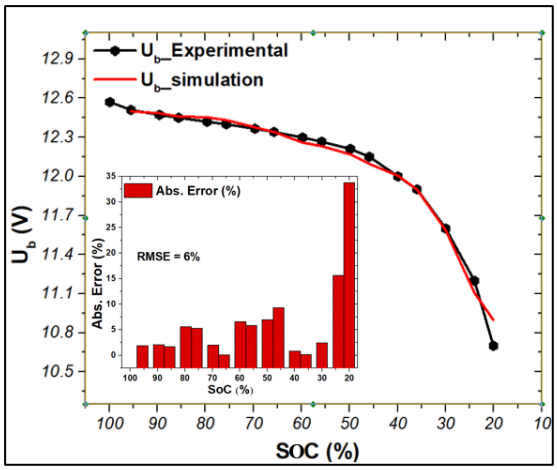

Figure 11: Validation results of improved Thévenin model.

To overcome the limitation of the improved Thévenin model at the low SOC region, a series capacitance is added to create what is known as the PNGV model.

4.6. Validation of the PNGV model

The second model is the PNGV model depicted in Figure 3, which includes a large series capacitance (C_o) incorporated to the improved Thévenin model. The series capacitance is representing the distinction between stored/drained charges which impacts the internal voltage based on U_{co} and capacity components. The terminal battery model for discharging process is expressed as follows:

$$U_b = U_{oc} - I_b R_o - U_{ov} - U_{co} \quad (15)$$

4.6.1. Estimation of model parameters

U_{oc}, R_o and **R//C** are common parameters in both the improved Thévenin and the PNGV models, consequently; only C_o will be estimated herein.

4.6.1.1. Series capacitance identification (C_o)

This ECM introduces a novel approach to modeling voltage fluctuations during battery cycling caused by variation of the amount of charges, by means of an ideal capacitor. Unlike previous models that utilized constant or controlled voltage sources, this model incorporates the limitations of real battery capacity by introducing an ideal capacitor in series with a constant ideal voltage source. The value of this capacitance (C_o) represents the slope between charge variation (ΔQ) and voltage (ΔU), which can be calculated according to equation 16.

$$\mathbf{C_o = \frac{\Delta Q}{\Delta U_{co}} = \frac{I_b \Delta t}{\Delta U_{co}}} \quad (16)$$

In this study, ΔQ is expressed as the product of multiplying the battery current (I_b = 10 A) and the time span along which the current is applied (Δt= 900 s). The value of ΔU_{oc} is evaluated by calculating the difference of voltages between two consecutive pulses, involving the battery recovery [14]. Figure 12 displays the extracted values of C_o at different SOC from the pulse discharge curve. These values exhibit a decreasing trend upon discharging and regression (f (SOC) equation that can be derived through nonlinear fitting as follows [14].

$$\mathbf{C_o = 1124000 - \frac{1060500}{\left(1 + \left(\frac{SOC}{36,8}\right)^{29,2}\right)^{0,072}}} \quad (17)$$

$$\mathbf{U_{co} = \frac{I_b, \Delta t}{C_o}} \quad (18)$$

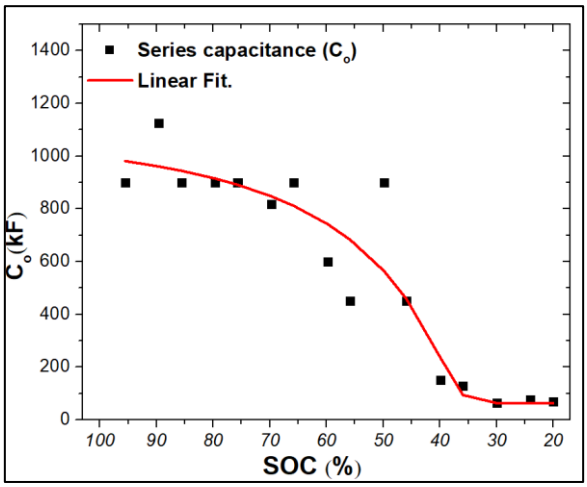

Figure 12: Variation of series capacitance (C_o) at different SOC.

4.6.2. Validation of PNGV model

Figure 13 shows the comparison between the simulated terminal voltage (**U_b**) and the actual discharge experimental data as a validation result of PNGV battery model. The experimental values were remarkably approximated by fitting equations that are dependent on SOC which were incorporated into the simulation model. The validation of model matches the experimental results ensuring its accuracy and reliability much better than the improved Thévenin model. PNGV is able to signify the battery Ohmic voltage drop, the transient voltage of diffusion and charge transfer processes and the variation of the internal battery voltage upon cycling due to SOC changes. The absolute error is presented in the inset insides, and the root-mean-square error this model is around **3%**.

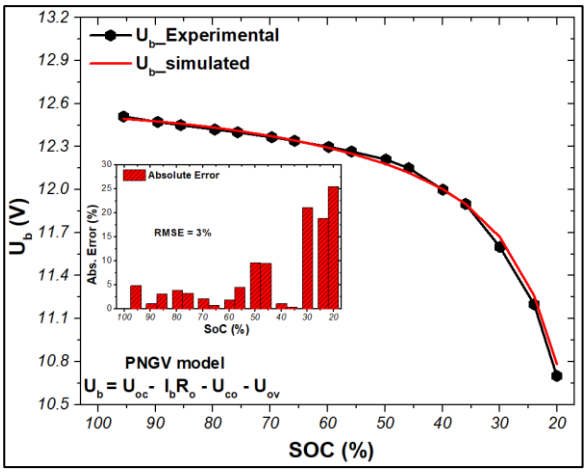

Figure 13: Validation results of the PNGV ECM showing the simulated terminal voltage (U_b) compared with the discharge experimental data at C/20/10 A.

5. Conclusion:

This paper has presented a comparative study of two different equivalent circuit models: the improved Thévenin model and the Partnership for a New Generation of Vehicle (PNGV) model. The modeling process began with a detailed analysis of experimental discharge tests. Data from pulsed discharge tests were used to obtain each battery model's parameters across a wide state of charge performance range. While the enhanced Thévenin model successfully simulated the overall battery behavior, its accuracy was notably compromised, particularly at lower states of charge. Conversely, the PNGV model was able to simulate the actual battery response with excellent accuracy. The PNGV model was successfully verified through practical testing, simulating the discharge voltage of the battery across its entire state of charge range with low error (RMSE ≈3 %). This emphasizes the PNGV model's superior performance, especially in comparison to the Thévenin model, which faced challenges specifically in accurately representing lower state of charge values. Consequently, adding a large series capacitor considerably enhanced the model topology, signifying its reliability despite extensive variations in current and voltage.

6. Nomenclature

PNGV model	The Partnership for a New Generation of Vehicle model
RMSE	Root mean square error percent
PV systems	Photovoltaic systems
SLA batteries	Sealed lead-acid batteries
VRLA batteries	Valve-regulated lead-acid batteries
ECMs	Equivalent circuit models
SOC	Battery's state of charge
AC	Alternative current
I_{sc}	Short circuit current of PV
V_{oc}	Open circuit voltage of PV
R_{sd}	Self-discharge resistance
I_{sd}	Self-discharge current
τ	Time constant
U_b	Battery discharge voltage
U_{OC}	Battery open-circuit voltage
R_o	Internal resistance
C_o	Series capacitor
C_n	Nominal capacity
I_b	Battery current
$R_{ov}//C_{ov}$	Parallel capacitor-resistor combination

7. Conflicts of interest

The authors declare that they have no conflict of interest in this article.

8. Acknowledgments

E. T. El Shenawy acknowledges the financial support of this work by the National Research Centre project (13040111).

9. References

[1] A. Mahjoob, P. Ahmadi, H. Afsaneh, M. Vojdani, and M. Mortazavi, 'System sizing and transient simulation of a solar photovoltaic off-grid energy system in various climates with air heat pumps', Sustainable Energy Technologies and Assessments, 54 (2022) 102788, doi: 10.1016/J.SETA.2022.102788.

[2] P. Kosky, R. Balmer, W. Keat, and G. Wise, 'Green Energy Engineering', in Exploring Engineering (Fifth Edition) An Introduction to Engineering and Design, Elsevier,(2021) pp. 431–452. doi: 10.1016/b978-0-12-815073-3.00019-3.

[3] T. M. Letcher, 'Storing electrical energy', in Managing Global Warming: An Interface of Technology and Human Issues, Elsevier Inc., (2019) 365–377. doi: 10.1016/B978-0-12-814104-5.00011-9.

[4] A. Mansuroglu, M. Gencten, M. B. Arvas, M. Sahin, and Y. Sahin, 'Investigation the effects of chlorine doped graphene oxide as an electrolyte additive for gel type valve regulated lead acid batteries', J Energy Storage, 64 (2023) 107224, doi: 10.1016/j.est.2023.107224.

[5] J. Díaz-Pilpe et al., 'Methodology for the third-party reconditioning process of automotive vented lead-acid (VLA) batteries', Procedia CIRP, 118 (2023) 970–975, doi: 10.1016/j.procir.2023.06.167.

[6] M. Mohsin, A. Picot, and P. Maussion, 'A new lead-acid battery state-of-health evaluation method using

electrochemical impedance spectroscopy for second life in rural electrification systems', J Energy Storage, 52 (2022) 104647, doi: 10.1016/j.est.2022.104647.

[7] P. Tsafack, S. E. Fru, A. V. Nghemachi, and E. Tanyi, 'Impact of high constant charging current rates on the charge/discharge efficiency in lead acid batteries, for residential photovoltaic system applications', J Energy Storage, 63 (2023) 107013, doi: 10.1016/j.est.2023.107013.

[8] E. D. Festijo, D. E. O. Juanico, P. V. Nonat, X. Galapia, and K. M. S. Malab, 'Acoustic non-invasive estimation of lead–acid battery state of health: Applications for cell-level charge balancing', Energy Reports, 8(2022) 372–377, doi: 10.1016/j.egyr.2022.10.242.

[9] Z. P. Nodeh, A. A. Beni, and A. J. Moghadam, 'Development of evaporation technique for concentrating lead acid wastewater from the battery recycling plant, by nanocomposite ceramic substrates and solar/wind energy', J Environ Manage, 328(2023)116980, doi:10.1016/j.jenvman.2022.116980.

[10] I. Pvps, 'Task 3: Lead-Acid Battery Guide for Stand-Alone Photovoltaic Systems 991223', (1999) 1-33.

[11] M. Huck and D. U. Sauer, 'Modeling transient processes in lead-acid batteries in the time domain', J Energy Storage, vol. 29, no. January, p. 101430, 2020, doi: 10.1016/j.est.2020.101430.

[12] S. Sathiakumar, "An investigation on the suitable battery system for marine applications', School of Electrical and Information engineering, University of Sydney. Sydney (2006).

[13] M. Real, H.-P. Bader, and R. Scheidegger, 'Minimizing the environmental impact of large-scale rural PV', Renewable energy world, James and James (science publishers) Ltd London, 4 (1) (2001) 47–59.

[14] M. Bašic, D. Vukadinovic, V. Višnjic, and I. Rakic, 'Dynamic Equivalent Circuit Models of Lead-Acid Batteries - A Performance Comparison', in IFAC-Papers On Line, Elsevier B.V. (2022) 189–194. doi: 10.1016/j.ifacol.2022.06.031.

[15] W. Zhou, Y. Zheng, Z. Pan, and Q. Lu, 'Review on the Battery Model and SOC Estimation Method', Processes, 9 (9) (2021) 1685, doi: 10.3390/pr9091685.

[16] M. Dürr, A. Cruden, S. Gair, and J. R. McDonald, 'Dynamic model of a lead acid battery for use in a domestic fuel cell system', J Power Sources, 161 (2) (2006) 1400–1411, doi: 10.1016/j.jpowsour.2005.12.075.

[17] D. Berndt, Maintenance-Free Batteries: Lead-Acid, Nickel/Cadmium, Nickel/Metal Hydride (Electronic & Electrical Engineering Research Studies), 2nd Edition. 1997.

[18] M. Franke and J. Kowal, 'Empirical sulfation model for valve-regulated lead-acid batteries under cycling operation', J Power Sources, 380 (2018) 76–82, doi: 10.1016/j.jpowsour.2018.01.053.

[19] J. Timmermans, R. Gopalakrishnan, O. Capron, A. Nikolian, J. De Hoog, T. Coosemans, N. Omar and J. Van Mierlo, 'Towards competitive European batteries How to model a battery, is a source and a resistor enough?' in Workshop EPE Conference, Geneva, 2015.

[20] M. Tomasov, M. Kajanova, P. Bracinik, and D. Motyka, 'Overview of battery models for sustainable power and transport applications', Transportation Research Procedia, 40 (2019) 548–555, 2019, doi: 10.1016/j.trpro.2019.07.079.

[21] A. S. Pande, B. P. Soni, and K. V. Bhadane, 'Electrical Models for EV's Batteries: An Overview and Mathematical Design of RC Network', Journal of The Institution of Engineers (India): Series B, 104 (2) (2023) 533–547, doi: 10.1007/s40031-022-00852-1.

[22] S. Lavety, R. K. Keshri, and M. A. Chaudhari, 'A dynamic battery model and parameter extraction for discharge behavior of a valve regulated lead-acid battery', J Energy Storage, 33 (2021) 102031, doi: 10.1016/j.est.2020.102031.

[23] M. Shi, J. Yuan, L. Dong, D. Zhang, A. Li, and J. Zhang, 'Combining physicochemical model with the equivalent circuit model for performance prediction and optimization of lead-acid batteries', Electrochim Acta, 353 (2020) 136567, doi: 10.1016/j.electacta.2020.136567.

[24] H. E. A. Chacón, E. Banguero, A. Correcher, Á. Pérez-Navarro, and F. Morant, "Modelling, parameter identification, and experimental validation of a lead acid battery bank using evolutionary algorithms", Energies, 11 (9) (2018), doi: 10.3390/en11092361.

[25] B. S. Kaloko and M. H. Purnomo, "Estimation of Residual Capacity of Lead Acid Battery using RBF Model," Int J Comput Appl, Special Issue on Artificial Intelligence Techniques - Novel Approaches & Practical Applications, 3 (2011) 12–17. Published by Foundation of Computer Science.

[26] A. Ganesan and S. Sundaram, "A Heuristic Algorithm for Determining State of Charge of a Lead Acid Battery for Small Engine Applications," SAE Technical Paper 2012-32-0082 (2012), doi: 10.4271/2012-32-0082.

[27] H. Fang, X. Zhao, Y. Wang, Z. Sahinoglu, T. Wada, S. Hara, R. A. de Callafon, 'State-of-charge estimation for batteries: A multi-model approach', in 2014 American Control Conference, IEEE, (2014) 2779–2785. doi: 10.1109/ACC.2014.6858976.

[28] F. Coupan, I. Sadli, I. Marie-Joseph, A. Primerose, and H. Clergeot, 'New battery dynamic model: Application to lead-acid battery', in 2010 The 2nd International Conference on Computer and Automation Engineering (ICCAE), IEEE, (2010) 140–145. doi: 10.1109/ICCAE.2010.5451494.

[29] Z. M. Salameh, M. A. Casacca, and W. A. Lynch, 'A mathematical model for lead-acid batteries', IEEE Transactions on Energy Conversion, 7 (1) (1992) 93–98, doi: 10.1109/60.124547.

[30] M. Bruch, L. Millet, J. Kowal, and M. Vetter, 'Novel method for the parameterization of a reliable equivalent circuit model for the precise simulation of a battery cell's electric behavior', J Power Sources, 490 (2021) 229513,

doi: 10.1016/j.jpowsour.2021.229513.

[31] Y. H. Kirn and H. D. Ha, 'Design of interface circuits with electrical battery models', IEEE Transactions on Industrial Electronics, 44(1) (1997) 81–86, doi: 10.1109/41.557502.

[32] N. Jantharamin and L. Zhang, 'A new dynamic model for lead-acid batteries', in 4th IET International Conference on Power Electronics, Machines and Drives (PEMD 2008), IEE, (2008) 86–90. doi: 10.1049/cp:20080488.

[33] R. Haddad, A. El Shahat, and Y. Kalaani, 'Lead Acid Battery Modeling for PV Applications', Journal of Electrical Engineering, 15(2) (2015) 17–24.

[34] Y. Hu, S. Yurkovich, Y. Guezennec, and B. J. Yurkovich, 'A technique for dynamic battery model identification in automotive applications using linear parameter varying structures', Control Eng. Pract. 17 (10) (2009) 1190–1201, doi: 10.1016/j.conengprac.2009.05.002.

[35] A. Li, S. Pelissier, P. Venet, and P. Gyan, 'Fast Characterization Method for Modeling Battery Relaxation Voltage', Batteries, 2 (2) (2016) 7, doi: 10.3390/batteries2020007.

[36] S. Jiang, "A Parameter Identification Method for a Battery Equivalent Circuit Model", SAE Technical Paper 2011-01-1367, 2011, https://doi.org/10.4271/2011-01-1367.

[37] S. Castano, L. Gauchia, E. Voncila, and J. Sanz, 'Dynamical modeling procedure of a Li-ion battery pack suitable for real-time applications', Energy Convers Manag, 92 (2015) 396–405, doi: 10.1016/j.enconman.2014.12.076.

[38] http://www.sonnenschein.org/A400.htm, 'A 400 sonnnschein battery website'. Accessed: Sep. 09, 2023. http://www.sonnenschein.org/A400.htm